V European Conference on Computational Fluid Dynamics
ECCOMAS CFD 2010
J. C. F. Pereira and A. Sequeira (Eds)
Lisbon, Portugal,14-17 June 2010

NUMERICAL TESTS OF A NEW PRESSURE CORRECTION SCHEME FOR THE HOMOGENEOUS MODEL (ECCOMAS CFD 2010)

W. Kheriji[*†], R. Herbin[*] and J.-C. Latché[†]

[*]Université de Provence,
e-mail: {kheriji, herbin}@cmi.univ-mrs.fr
[†]Institut de Radioprotection et de Sûreté Nucléaire (IRSN)
e-mail: {walid.kheriji, jean-claude.latche}@irsn.fr

Key words: Two-phase flows, homogeneous model, pressure correction schemes, finite volumes, finite elements, Riemann problems, Shock tube problems

Abstract. *We assess in this paper the capability of a pressure correction scheme to compute irregular solutions (*i.e. *solutions with shocks) of the homogeneous model for barotropic two-phase flows. This scheme is designed to inherit the stability properties of the continuous problem: the unknowns (in particular the density and the mass fraction y of the dispersed phase) are kept within their physical bounds, and the entropy of the system is conserved, thus providing and unconditional stability property. In addition, the scheme keeps the velocity and pressure constant through contact discontinuities (which, here, are discontinuities of y like, for instance, a gas/liquid interface). To this aim, the mass balance and the transport equation for y are coupled in an original pressure correction step. The space discretization is staggered, using either the Marker-And Cell (MAC) scheme or nonconforming low-order finite element approximations; in either case, finite volume techniques are used for all the convection terms. Numerical experiments performed here address the solution of various Riemann problems, often called in this context "shock tube problems". They show that, provided that a sufficient numerical dissipation is introduced in the scheme, it converges to the (weak) solution to the continuous problem. Observed orders of convergence as a function of the mesh and time step at constant CFL number vary with the studied cases and the CFL number, and range from* 0.5 *to* 1.5 *for the velocity and the pressure; in most cases, the density and y converge with a* 0.5 *order. Finally, the scheme shoes a satisfactory behaviour up to CFL numbers far greater than 1.*

1 INTRODUCTION

We consider in this paper a perturbation of the non-viscous homogeneous two-phase flow model, let say a liquid phase and a gas phase, which reads:

$$\partial_t \rho + \mathrm{div}(\rho\, \boldsymbol{u}) = 0, \tag{1}$$
$$\partial_t z + \mathrm{div}(z\, \boldsymbol{u}) = 0, \tag{2}$$
$$\partial_t(\rho\, \boldsymbol{u}) + \mathrm{div}(\rho\, \boldsymbol{u} \otimes \boldsymbol{u}) + \nabla p - \mu\, (\Delta \boldsymbol{u} + \frac{1}{3}\nabla \mathrm{div} \boldsymbol{u}) = 0, \tag{3}$$

where ∂_t is the time derivative, ρ, $\boldsymbol{u}$ and p are the (average) density, velocity and pressure in the flow, z stands for the partial density of the gas phase and μ is a small positive parameter. The problem is defined over an open bounded connected subset Ω of $\mathbb{R}^d$, $d \leq 3$, and over a finite time interval $(0, T)$. We suppose that suitable initial and boundary conditions are provided for ρ, $\boldsymbol{u}$ and z ; in particular, the prescribed values for ρ and z are supposed to be positive, and ρ, $\boldsymbol{u}$ and z are supposed to be prescribed at the inflow boundaries. The first two equations, (1) and (2), are the mixture and the gas mass balance, respectively, and the third equation (3) is the mixture momentum balance. The density of the fluid ρ is supposed to be given by:

$$\rho = (1-\alpha)\, \rho_\ell + \alpha\, \rho_g, \quad \alpha = \frac{z}{\rho_g} \qquad \text{or} \quad \rho = \frac{1}{\dfrac{y}{\rho_g} + \dfrac{1-y}{\rho_\ell}}, \tag{4}$$

where ρ_g and ρ_ℓ are the phasic (gas and liquid, respectively) densities, α is called the void fraction (the volume of gas per specific volume), and $y = z/\rho$ is the gas mass fraction (the gas mass per specific mass). We suppose that the flow is barotropic (*i.e.* that the phasic densities depend on the pressure only), and, more precisely, that ρ_ℓ is constant and ρ_g is given by a function of the pressure:

$$\rho_g = \varrho_g(p), \tag{5}$$

where ϱ is defined and increasing over $[0, +\infty)$, $\varrho(0) = 0$ and $\lim_{s \to +\infty} \rho(s) = +\infty$.

We now recall some estimates which are satisfied, at least formally, by the solution of System (1)-(3). Equation (1) shows that ρ remains non-negative at all time. Replacing y by its definition in the gas mass balance (2) and using the mass balance (1), we get:

$$\partial_t(\rho y) + \nabla \cdot (\rho y\, \boldsymbol{u}) = \rho\, \left(\partial_t y + \boldsymbol{u} \cdot \nabla y\right) = 0.$$

Let us suppose that ρ does not vanish (which is not necessarily true at the continuous level, since div$\boldsymbol{u}$ is not bounded in $\mathrm{L}^\infty(\Omega)$, but will be true at the discrete level). Then this relation implies that y satisfies a maximum principle. So, if the initial and boundary conditions for ρ and z are such that $y \in [\varepsilon, 1]$ at $t = 0$, where $0 < \varepsilon \leq 1$ (which excludes

purely liquid zones at the initial time), we obtain that y remains in the interval $[\varepsilon, 1]$ at all times. From the second form of (4) and the fact that $\rho > 0$, we can deduce that $\rho \in [\min(\rho_\ell, \rho_g), \max(\rho_\ell, \rho_g)]$ and, now from the first form of (4), $\alpha \in (0, 1]$, so $\rho_g > 0$ and, since ϱ_g is one-to-one from $(0, +\infty)$ to itself, the pressure p is well defined and positive.

Let us now define the function $\mathcal{P}$, from $(0, +\infty)$ to $\mathbb{R}$, as a primitive of $s \mapsto \wp_g(s)/s^2$, where $\wp_g = \varrho_g^{-1}$. Then, if we suppose that the velocity is prescribed to zero at the boundary, the solution to System (1)-(3) satisfies:

$$\frac{d}{dt} \int_\Omega \left[\frac{1}{2} \rho \left|\boldsymbol{u}\right|^2 + z\mathcal{P}(\varrho_g(p))\right] \mathrm{d}\boldsymbol{x} \leq 0. \tag{6}$$

The quantity $z\mathcal{P}(\varrho_g(p))$ is often called the Helmotz energy, $\frac{1}{2} \rho \left|\boldsymbol{u}\right|^2$ the kinetic energy and their sum is the total energy of the system. Since the function $\mathcal{P}$ is increasing, Inequality (6) provides an estimate on the solution.

When $\mu = 0$, System (1)-(3) is hyperbolic, with a well-known wave structure. Solution to Riemann problems always involves a contact discontinuity, and two additional waves, which are either shock or rarefaction waves. Through the contact discontinuity, the pressure and velocity are kept constant, and z, ρ or y are discontinuous. The existence of this wave may be inferred by just checking that, provided this is consistent with initial and boundary conditions, a solution to the system with constant velocity and pressure exists: indeed, from the first form of (4), it may be seen that ρ and z are linked by an affine relation with constant (with a constant pressure) coefficients; (1) and (2) then boil down to the same transport equation (with a constant velocity) and (3) is trivially satisfied.

The use of pressure correction schemes for single phase flow, even without theoretical bound, seems to be widespread (see *e.g.* [6] for the seminal work and [14] for a comprehensive introduction), because this kind of scheme, usually partly implicit, preserve some stability with respect to the time step together with introducing a decoupling of the equations sufficient to hope to solve the nonlinear sytems produced by the scheme. Extensions to multi-phase flows are scarcer, and seem to be restricted to iterative algorithms, often similar in spirit to the usual SIMPLE algorithm for incompressible flows [13, 10, 8]. In this paper, we perform a numerical study of a non-iterative pressure-correction scheme introduced in [4] which enjoys the following properties:

- (*i*) the scheme has at least one solution, and any solution satisfies the "discrete-maximum-based" estimates listed above: $\rho > 0$, the gas mass fraction y satisfies a discrete maximum principle, and $p > 0$.
- (*ii*) the scheme is unconditionally stable, in the sense that its solution(s) satisfy a discrete analogue of Inequality (6),
- (*iii*) the pressure and velocity are kept constant through contact discontinuities.

In addition, the scheme is conservative for ρ and z. It boils down to the usual projection scheme for incompressible flows (obtained in the present framework when $y = 0$ or, asymptotically, when the function ϱ_g varies more and more slowly). Its accuracy was assessed for smooth solutions in [4].

The aim of the present paper is to check the convergence and accuracy of this scheme for weak solutions with discontinuities. It is organized as follows. We first present the scheme (Section 2). Then we compute various Riemann problems, first monophasic ($y = 1$) (Section 3.1) then diphasic: we address first a flow involving only a contact discontinuity and shocks (Section 3.2.1), and finally a flow with rarefaction waves (Section 3.2.2).

2 THE SCHEME

2.1 Time semi-discretization

Let us consider a partition $0 = t_0 < t_1 < \ldots < t_N = T$ of the time interval $(0, T)$, which is supposed uniform for the sake of simplicity. Let $\delta t = t_{n+1} - t_n$ for $n = 0, 1, \ldots, N-1$ be the constant time step. In a time semi-discrete setting, denoting by ρ^{-1} and u^0 initial guesses for the density and velocity, the algorithm proposed in this paper is the following.

0 - Initialization – Compute ρ^0 by solving :

$$\frac{\rho^0 - \rho^{-1}}{\delta t} + \mathrm{div}(\rho^0 \boldsymbol{u}^0) = 0. \tag{7}$$

Then, for $n \geq 0$:

1 - Prediction step – Solve for $\tilde{\boldsymbol{u}}^{n+1}$:

$$\frac{\rho^n\ \tilde{\boldsymbol{u}}^{n+1} - \rho^{n-1}\ \boldsymbol{u}^n}{\delta t} + \mathrm{div}(\rho^n\ \boldsymbol{u}^n \otimes \tilde{\boldsymbol{u}}^{n+1}) + \nabla p^n - \mu\left(\Delta \tilde{\boldsymbol{u}}^{n+1} + \frac{1}{3}\nabla \mathrm{div} \tilde{\boldsymbol{u}}^{n+1}\right) = 0. \tag{8}$$

2 - Pressure correction step – Solve for p^{n+1}, $\boldsymbol{u}^{n+1}$, ρ^{n+1} and z^{n+1}

$$\rho^n\ \frac{\boldsymbol{u}^{n+1} - \tilde{\boldsymbol{u}}^{n+1}}{\delta t} + \nabla(p^{n+1} - p^n) = 0, \tag{9a}$$

$$\frac{\rho^{n+1} - \rho^n}{\delta t} + \mathrm{div}(\rho^{n+1}\ \boldsymbol{u}^{n+1}) = 0, \tag{9b}$$

$$\frac{z^{n+1} - z^n}{\delta t} + \mathrm{div}(z^{n+1}\ \boldsymbol{u}^{n+1}) = 0, \tag{9c}$$

$$\rho^{n+1} = \varrho(p^{n+1}, z^{n+1}). \tag{9d}$$

Step 1 is the usual prediction step for the velocity, which consists in solving the momentum balance equation with the beginning-of-step pressure. Step 2 is the pressure correction step. For its solution, Equations (9a) and (9b) are combined to obtain a non-linear elliptic problem for the pressure, which reads in the time semi-discrete setting:

$$\frac{\rho^{n+1}-\rho^n}{\delta t^2} - \mathrm{div}\Big[\frac{\rho^{n+1}}{\rho^n}\nabla(p^{n+1}-p^n)\Big] = -\frac{1}{\delta t}\,\mathrm{div}(\rho^{n+1}\tilde{u}^{n+1}), \qquad \text{with } \rho^{n+1} = \varrho(p^{n+1}, z^{n+1}). \tag{10}$$

Note that, with the space discretization chosen here, this equations must be established by making the manipulations necessary to derive it (*i.e.* multipplying the first equation by ρ^{n+1}/ρ^n, taking its divergence and substracting to the second relation) at the algebraic level [4].

Two things are unusual in this algorithm. The first one is the time-shift of the densities in the prediction step; its motivation lies in the fact that it is necessary for the convection operator to vanish for constant velocities (*i.e.* $\tilde{u}^{n+1} = 1$) to ensure the conservation of the kinetic energy [3, 1]. Second, the pressure correction step, in a rather unusual way, couples the mixture and dispersed phase mass balance; this coupling preserves the affine relation between ρ^{n+1} and z^{n+1} through the equation of state, with coefficient only depending on the pressure (taken at the same time level). Thus, as in the continuous case, both equations boil down to only one relation when the pressure is constant; consequently, the arguments necessary to obtain solutions with constant velocity and pressure (*i.e.* contact discontinuity waves) still hold at the discrete level.

2.2 Discrete spaces and unknowns

The scheme has been developped (and actually works) with unstructured (in particular simplicial) discretizations, and for 2D and 3D cases. However, since our aim here is to solve 1D Riemann problems, wo choose, for the sake of conciseness, to only describe the case of 2D structured meshes. For the same reasons, we restrict the presentation to the Rannacher-Turek element, but a finite volume MAC discretization would also be implemented.

Let $\mathcal{M}$ be a decomposition of the domain Ω into rectangles, supposed to be regular in the usual sense of the finite element literature (e.g. [2]). By $\mathcal{E}$ and $\mathcal{E}(K)$ we denote the set of all edges σ of the mesh and of the element $K \in \mathcal{M}$ respectively. The set of edges included in the boundary of Ω is denoted by $\mathcal{E}_{\rm ext}$ and the set of internal ones (*i.e.* $\mathcal{E} \setminus \mathcal{E}_{\rm ext}$) is denoted by $\mathcal{E}_{\rm int}$. For each internal edge of the mesh $\sigma = K|L$, $\boldsymbol{n}_{KL}$ stands for the normal vector to σ, oriented from K to L. By $|K|$ and $|\sigma|$ we denote the measure, respectively, of the control volume K and of the edge σ.

The velocity and the pressure are discretized using the so-called Rannacher and Turek element [12]. The approximation for the velocity is thus non-conforming (discrete functions are discontinuous through an edge, but the jump of their integral is imposed to be

zero), the degrees of freedom are located at the center of the edges of the mesh, and we choose the version of the element where they represent the average of the velocity through an edge. The set of degrees of freedom reads:

$$\{\boldsymbol{u}_{\sigma,i},\ \sigma \in \mathcal{E},\ 1 \leq i \leq d\}.$$

We denote by $\boldsymbol{\varphi}_\sigma^{(i)}$ the vector shape function associated to $\boldsymbol{u}_{\sigma,i}$, which, by definition, reads $\boldsymbol{\varphi}_\sigma^{(i)} = \varphi_\sigma\, \boldsymbol{e}^{(i)}$, where φ_σ is the Rannacher-Turek scalar shape function and $\boldsymbol{e}^{(i)}$ is the i^{th} vector of the canonical basis of $\mathbb{R}^d$, and we define $\boldsymbol{u}_\sigma$ by $\boldsymbol{u}_\sigma = \sum_{i=1}^d \boldsymbol{u}_{\sigma,i}\, \boldsymbol{e}^{(i)}$. With these definitions, we have the identity:

$$\boldsymbol{u} = \sum_{\sigma\in\mathcal{E}} \sum_{i=1}^{d} \boldsymbol{u}_{\sigma,i}\ \boldsymbol{\varphi}_\sigma^{(i)}(\boldsymbol{x}) = \sum_{\sigma\in\mathcal{E}} \boldsymbol{u}_\sigma\ \varphi_\sigma(\boldsymbol{x}), \qquad \text{for a.e. } \boldsymbol{x} \in \Omega.$$

Let $\mathcal{E}_D \subset \mathcal{E}_{\text{ext}}$ be the set of edges where the velocity is prescribed, let say to $\boldsymbol{u} = \boldsymbol{u}_D$. Then, as usual, these Dirichlet boundary conditions are built-in in the definition of the discrete space:

$$\forall \sigma \in \mathcal{E}_D,\ \text{for } 1 \leq i \leq d, \qquad \boldsymbol{u}_{\sigma,i} = \frac{1}{|\sigma|} \int_\sigma \boldsymbol{u}_{D,i},$$

where $\boldsymbol{u}_{D,i}$ stands for the i^{th} component of $\boldsymbol{u}_D$.

The pressure, and the other variables ρ, y and z are piecewise constant, and their degrees of freedom are:

$$\{p_K,\ \rho_K,\ y_K \text{ and } z_K,\ K \in \mathcal{M}\}.$$

2.3 Space discretization

We now describe the space discretization of each equation of the time semi-discrete algorithm, and choose to present the equations of the projection step in their original form, *i.e.* before the derivation of the elliptic problem for the pressure, which may be found in [4]. Indeed, note that this operation is purely algebraic, in the sense that it transforms a nonlinear algebraic system into another nonlinear algebraic system which is strictly equivalent to the first one, and thus has no impact on the properties of the scheme (besides, of course, the efficiency issue).

We begin with the mass balances, *i.e.* the second and third equations the projection step. The are obtained by an upwind finite volume discretization of (9b):

$$\forall K \in \mathcal{M}, \qquad \begin{aligned} &\frac{|K|}{\delta t}\,(\rho_K^{n+1} - \rho_K^n) + \sum_{\sigma\in\mathcal{E}(K)} |\sigma|\ \boldsymbol{u}_\sigma^{n+1}\cdot\boldsymbol{n}_\sigma\ \rho_\sigma^{n+1} = 0, \\ &\frac{|K|}{\delta t}\,(z_K^{n+1} - z_K^n) + \sum_{\sigma\in\mathcal{E}(K)} |\sigma|\ \boldsymbol{u}_\sigma^{n+1}\cdot\boldsymbol{n}_\sigma\ z_\sigma^{n+1} = 0, \end{aligned} \tag{11}$$

where ρ_σ^{n+1} (resp. z_σ^{n+1}) is the upwind approximation of ρ^{n+1} (resp. z^{n+1}) at the edge σ, the definition of which we now recall for the sake of completeness. For an internal edge $\sigma = K|L$, ρ_σ^{n+1} (resp. z_σ^{n+1}) stands for ρ_K^{n+1} (resp. z_K^{n+1}) if $\boldsymbol{u}_\sigma^{n+1} \cdot \boldsymbol{n}_\sigma \geq 0$ and for ρ_L^{n+1} (resp. z_L^{n+1}) otherwise; for an external edge $\sigma \in \mathcal{E}(K)$, ρ_σ^{n+1} (resp. z_σ^{n+1}) is equal to ρ_K^{n+1} (resp. z_K^{n+1}) if the flow is directed outward Ω (*i.e.* $\boldsymbol{u}_\sigma^{n+1} \cdot \boldsymbol{n}_\sigma \geq 0$) or given by the boundary conditions otherwise. This approximation ensures that $\rho^{n+1} > 0$ as soon as $\rho^n > 0$ and the density is prescribed to a positive value at inflow boundaries. In addition, if we set $y_K^{n+1} = z_K^{n+1}/\rho_K^{n+1}$ and $y_K^n = z_K^n/\rho_K^n$, we may recast the second equation of (11) as:

$$\frac{|K|}{\delta t}\left(\rho_K^{n+1} y_K^{n+1} - \rho_K^n y_K^n\right) + \sum_{\sigma \in \mathcal{E}(K)} |\sigma|\ \boldsymbol{u}_\sigma^{n+1} \cdot \boldsymbol{n}_\sigma\ \rho_\sigma^{n+1} y_\sigma^{n+1} = 0, \tag{12}$$

where we recognize in y_σ^{n+1} the upwind approximation of y^{n+1} at the edge σ. This relation thus yields that y^{n+1} satisfies a discrete maximum principle by standard arguments [9].

The velocity prediction equation is approximated by a combination of a dual mesh finite volume technique, for the time derivative term and convection term and a finite element technique for the other terms. We define the dual mesh as follows. For any $K \in \mathcal{M}$ and any face $\sigma \in \mathcal{E}(K)$, let $D_{K,\sigma}$ be the cone of basis σ and of opposite vertex the mass center of K. The volume $D_{K,\sigma}$ is referred to as the half-diamond mesh associated to K and σ. For $\sigma \in \mathcal{E}_{\rm int}$, $\sigma = K|L$, we now define the diamond mesh D_σ associated to σ by $D_\sigma = D_{K,\sigma} \cup D_{L,\sigma}$; for an external edge $\sigma \in \mathcal{E}_{\rm ext} \cap \mathcal{E}(K)$, D_σ is just the same volume as $D_{K,\sigma}$. We denote by $\varepsilon = D_\sigma|D_{\sigma'}$ the face separating two diamond meshes D_σ and $D_{\sigma'}$ (see Figure 1).

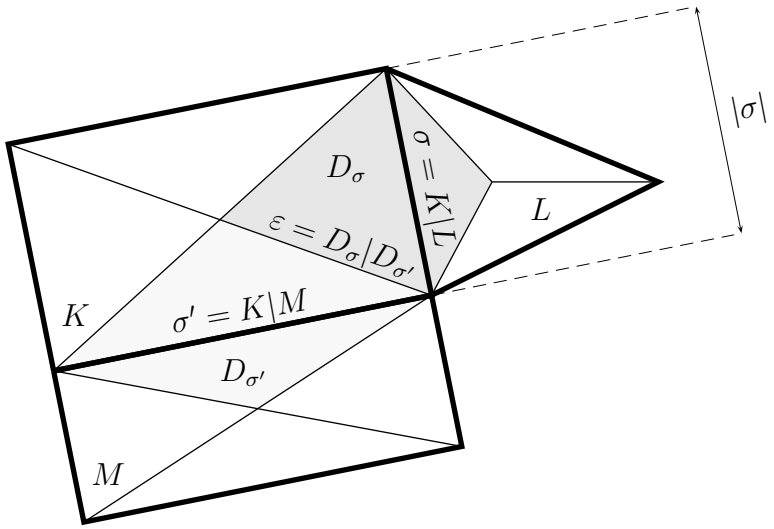

Figure 1: Notations for control volumes and diamond cells.

With these notations, the discretization of the momentum balance equation reads:

$$\begin{aligned}&\forall \sigma \in \mathcal{E} \setminus \mathcal{E}_D, \text{ for } 1 \leq i \leq d,\\ &\frac{|D_\sigma|}{\delta t}\,(\bar{\rho}_\sigma^n\ \tilde{\boldsymbol{u}}_{\sigma,i}^{n+1} - \bar{\rho}_\sigma^{n-1}\ \boldsymbol{u}_{\sigma,i}^n) + \sum_{\varepsilon\in\mathcal{E}(D_\sigma)} F_{\varepsilon,\sigma}^n\ \tilde{\boldsymbol{u}}_{\varepsilon,i}^{n+1} + \mu \sum_{K\in\mathcal{M}} \int_K \nabla \tilde{\boldsymbol{u}}^{n+1} \cdot \nabla \boldsymbol{\varphi}_\sigma^{(i)})\\ &\qquad + \frac{\mu}{3} \sum_{K\in\mathcal{M}} \int_K \operatorname{div} \tilde{\boldsymbol{u}}^{n+1}\ \operatorname{div} \boldsymbol{\varphi}_\sigma^{(i)} - \sum_{K\in\mathcal{M}} \int_K p^n\ \nabla\cdot \boldsymbol{\varphi}_\sigma^{(i)} = 0,\end{aligned} \tag{13}$$

where $\bar{\rho}_\sigma^n$ and $\bar{\rho}_\sigma^{n-1}$ stands for an approximation of the density on the edge σ at time t^n and t^{n-1} respectively (which must not be identified with the approximation of the density used in the mass balance and denoted by ρ_σ^n), $F_{\varepsilon,\sigma}^n$ is the discrete mass flux through the dual edge ε outward D_σ, and $\tilde{\boldsymbol{u}}_{\varepsilon,i}^{n+1}$ stands for an approximation of $\tilde{\boldsymbol{u}}_i^{n+1}$ on ε wich may be chosen centered or upwind. In the centered case, for an internal side $\varepsilon = D_\sigma|D_{\sigma'}$, we thus get $\tilde{\boldsymbol{u}}_{\varepsilon,i}^{n+1} = (\tilde{\boldsymbol{u}}_{\sigma,i}^{n+1} + \tilde{\boldsymbol{u}}_{\sigma',i}^{n+1})/2$ while, in the upwind case, we have $\tilde{\boldsymbol{u}}_{\varepsilon,i}^{n+1} = \tilde{\boldsymbol{u}}_{\sigma,i}^{n+1}$ if $F_{\varepsilon,\sigma}^n \geq 0$ and $\tilde{\boldsymbol{u}}_{\varepsilon,i}^{n+1} = \tilde{\boldsymbol{u}}_{\sigma',i}^{n+1}$ otherwise. The main motivation to implement a finite volume approximation for the first two terms is to obtain a discrete equivalent of the kinetic energy theorem, which holds in the case of homogeneus Dirichlet boundary conditions and reads:

$$\begin{aligned}&\sum_{\sigma\in\mathcal{E}_{\rm int}} \Big[\frac{|D_\sigma|}{\delta t}\,(\bar{\rho}_\sigma^n\ \tilde{\boldsymbol{u}}_\sigma^{n+1} - \bar{\rho}_\sigma^{n-1}\ \boldsymbol{u}_\sigma^n) + \sum_{\varepsilon\in\mathcal{E}(D_\sigma)} F_{\varepsilon,\sigma}^n\ \tilde{\boldsymbol{u}}_\varepsilon^{n+1}\Big] \cdot\ \boldsymbol{u}_\sigma \geq\\ &\qquad \frac{1}{2} \sum_{\sigma\in\mathcal{E}_{\rm int}} \frac{|D_\sigma|}{\delta t}\ \big[\bar{\varrho}_\sigma^n\ |\tilde{\boldsymbol{u}}_\sigma^{n+1}|^2 - \bar{\varrho}_\sigma^{n-1}\ |\boldsymbol{u}_\sigma^n|^2\big].\end{aligned} \tag{14}$$

For this result to be valid, the necessary condition is that the convection operator vanishes for a constant velocity, *i.e.* that the following discrete mass balance over the diamond cells is satisfied [1, 3]:

$$\forall \sigma \in \mathcal{E}_{\rm int}, \qquad \frac{|D_\sigma|}{\delta t}\,(\bar{\rho}_\sigma^n - \bar{\rho}_\sigma^{n-1}) + \sum_{\varepsilon\in\mathcal{E}(D_\sigma)} F_{\varepsilon,\sigma}^n = 0.$$

This governs the choice for the definition of the density approximation $\bar{\rho}_\sigma$ and the mass fluxes $F_{\varepsilon,\sigma}$. The density $\bar{\rho}_\sigma$ is defined by a weighted average: $\forall \sigma \in \mathcal{E}_{\rm int}$, $\sigma = K|L$, $|D_\sigma|\ \bar{\rho}_\sigma = |D_{K,\sigma}|\ \rho_K + |D_{L,\sigma}|\ \rho_L$ and $\forall \sigma \in \mathcal{E}_{\rm ext} \setminus \mathcal{E}_D$, $\sigma \in \mathcal{E}(K)$, $\bar{\rho}_\sigma = \rho_K$. The flux $F_{\varepsilon,\sigma}$ through the dual edge ε of the half diamond cell $D_{K,\sigma}$ is computed as the flux through ε of a constant divergence lifting of the mass fluxes through the edges of the primal cell K, *i.e.* the quantities $(|\sigma|\boldsymbol{u}_\sigma \cdot \boldsymbol{n}_\sigma\ \rho_\sigma)_{\sigma\in\mathcal{E}(K)}$ appearing in the discrete mass balance (11). For a detailed construction of this approximation, we refer to [1].

The discretization of (9a) is consistent with that of the momentum balance (13), *i.e.* we use a mass lumping technique for the unsteady term and a standard finite element

formulation for the gradient of the pressure increment:

$$\forall \sigma \in \mathcal{E}_{\rm int}, \text{ for } 1 \leq i \leq d,$$
$$\frac{|D_\sigma|}{\delta t} \bar{\rho}_\sigma^n \left(\boldsymbol{u}_{\sigma,i}^{n+1} - \tilde{\boldsymbol{u}}_{\sigma,i}^{n+1}\right) - \sum_{K \in \mathcal{M}} \int_K (p^{n+1} - p^n) \, \nabla \cdot \boldsymbol{\varphi}_\sigma^{(i)} \, dx = 0.$$

3 NUMERICAl EXPERIMENTS

In this section, we assess the behaviour of the scheme, for various Riemann problems (often called also "shock tube problems"), the solution of which can be computed analytically. These problems are hyperbolic (*i.e.* the system of PDES is (1)-(3) with $\mu = 0$), monodimensional, and their initial solution is composed by two uniform states (the left (L) and right (R) states), separated by a discontinuity, located by convention at the origin $\boldsymbol{x} = 0$. We take benefit of the fact that the pressure correction scheme is able to keep $y = 1$ at any time, if the initial and boundary conditions allow it, to first begin with a single phase flow, namely the solution of the so-called "Sod shock tube" problem. Next, we turn to two-phase flows, namely "two-fluid shock tube" model problems.

The computations presented here are performed with the ISIS code [7], built from the software component library PELICANS [11], both under development at IRSN and available as free softwares. This computer code is devoted to the solution of 2D or 3D problems (as the scheme presented in previous sections), so we are lead to define an equivalent 2D problem, designed to boil down to the addressed 1D Riemann problem. The domain Ω is rectangular, and the mesh is composed of only one horizontal stripe of meshes (see Figure 2). We impose a symmetry condition to the velocity at the top and bottom of the domain Ω (i.e y-velocity $\boldsymbol{u}_y = 0$ and $\nabla \boldsymbol{u}_x \cdot \boldsymbol{t} = 0$, where $\boldsymbol{t}$ is a unit tangent vector to the boundary $\partial\Omega$), which is satisfied by a solution invariant with respect to the second coordinate. At the left side of the domain, we impose the value $(u_L, 0)$ to the velocity $\boldsymbol{u}$ and the value z_L to the partial gas density z. At the right side of the domain, we prescribe Neumann boundary condition, with a surface forcing term equal to $-p_R \, \boldsymbol{n}$, where $\boldsymbol{n}$ is the unit outward normal vector to the boundary $\partial\Omega$.

As described above, for the velocity convection term in the momentum balance equation, the approximation of the velocity at the edges of the dual mesh (see Figure 3) may be chosen centered or upwind; we will refer to the first option in the following as the centered cheme (even if upwinding is used in the discrete mass balances), and to the second one as the upwind scheme.

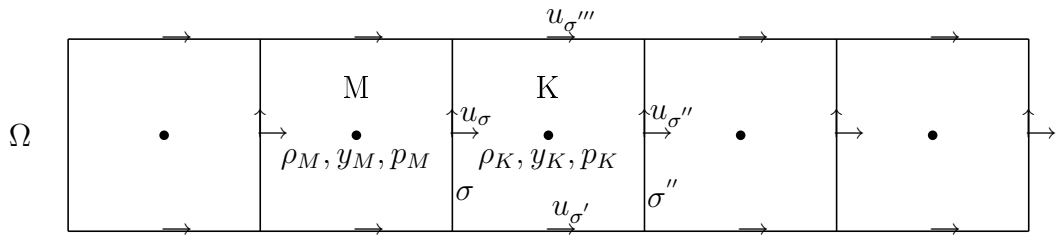

Figure 2: Rectangle finite volume mesh $\mathcal{M}$

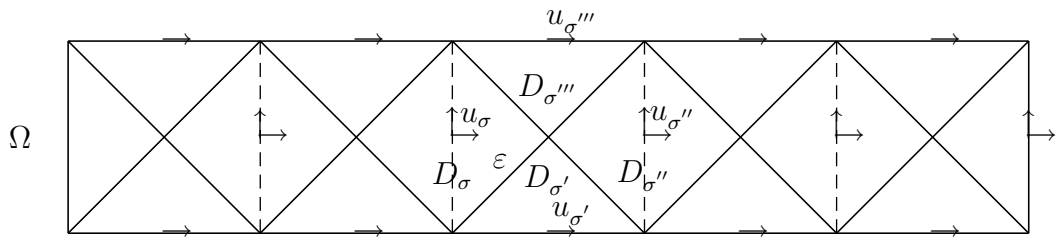

Figure 3: Dual finite volume mesh

3.1 Sod shock tube

We present here the numerical results for the well-known monophasic Sod shock tube; here, the (computed) gas mass fraction is $y \equiv 1$, which reduces the homogeneous model to the isothermal Euler equations. In this flow, the wave structure consists of a rarefaction wave travelling to the left and a shock travelling to the right. The (1D) continuous problem is posed over the interval $(-2, 3)$ and, for the computation, we take $\Omega = (-2, 3) \times [0, 0.01]$. The two initial constant states are given by:

$$\begin{pmatrix} \rho \\ \boldsymbol{u} \end{pmatrix}_L = \begin{pmatrix} 1 \\ 0 \end{pmatrix}, \qquad \begin{pmatrix} \rho \\ u \end{pmatrix}_R = \begin{pmatrix} 0.125 \\ 0 \end{pmatrix}.$$

The equation of state is given by $p = \rho RT$, the parameters R and T being adjusted to produce $RT = 1$.

Numerical experiments show that, as may be expected, the scheme does not seem to converge if we let $\mu = 0$ and the centered approximation in the momentum balance equation; indeed, we observe in this case, especially for the velocity, the usual odd-even decoupling characteristic of the behaviour of the centered scheme for the convection equation. For any other option, *i.e.* either if we keep an artificial residual viscosity or if we use the upwind approximation, convergence to the (weak) solution of the continuous problem seems to be achieved.

A numerical solution at $t = 1$ obtained with 2000 meshes, $\delta t = 0.00125$ and a residual viscosity of $\mu = 0.001$ is presented in Figure 4, together with the exact solution. Using $v = 1.6$ (which approximately corresponds to the velocity of the faster wave, namely the shock) as velocity range, these numerical parameters correspond to CFL$= v\ \delta t/h = 0.8$.

The influence of the artificial viscosity on the accuracy of the scheme is then checked. We observe on Figure 5 and Figure 6 that, as expected, taking too large viscosities yields inaccurate results, because the solved problem is too far from the original one, and that, with a too low value of the viscosity, the control on the solution is lost. In between, we observe a plateau, which shows that the accuracy of the scheme is rather robust with respect to the artificial viscosity. The optimal value for μ decreases with the time and space steps. Comparing Figures 5 and 6, we note that the plateau is wider for CFL=9.6, but the overall shape of the curves remains essentially similar for both CFL numbers.

We end this study by reporting the accuracy of the scheme as a function of the time and space step, with two constant CFL numbers, for the centered and upwind scheme; for the first option, the viscosity is given the constant value $\mu = 0.001$, and $\mu = 0$ (here and everywhere hereafter) for the upwind option.. For the centered scheme, the observed orders of convergence are about 0.5 and 1 at CFL=0.8 and 9.6 respectively, for both the velocity and the pressure. For the upwind scheme, the order of convergence is 0.75 in any case.

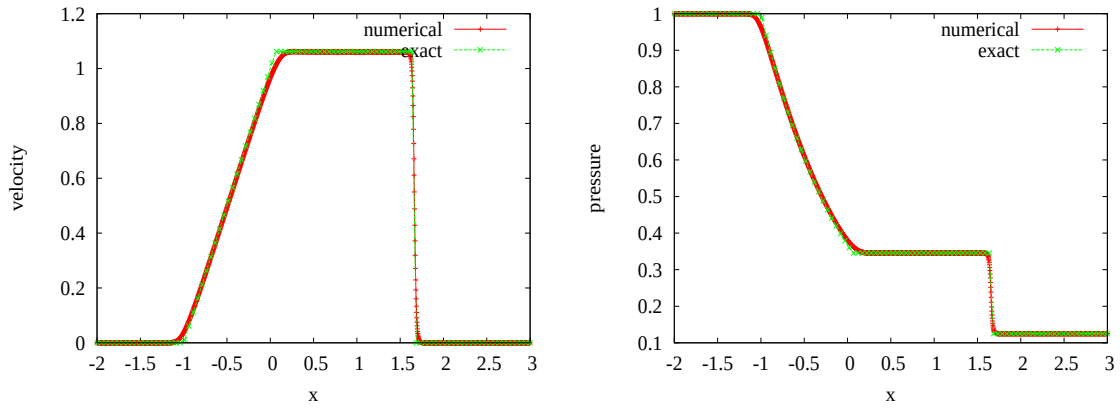

Figure 4: Sod shock tube problem - Numerical solution at $t = 1$ with the centered scheme ($\mu = 0.001$), 2000 meshes and $\delta t = 0.00125$ (*i.e.* CFL=0.8).

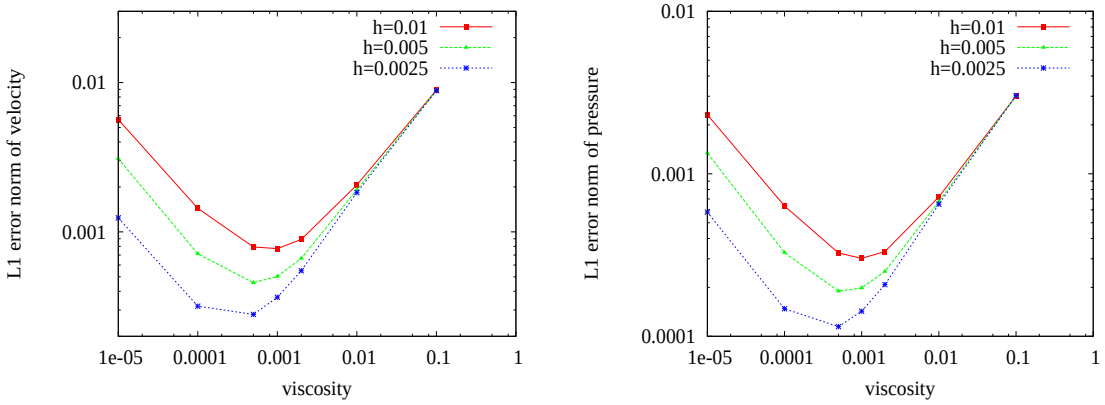

Figure 5: Sod shock tube problem - Error at $t = 1$, in L^1 norm (in space) for the velocity (left) and pressure (right) for three meshes, as a function of the artificial viscosity μ, with CFL= 0.8 (centered scheme).

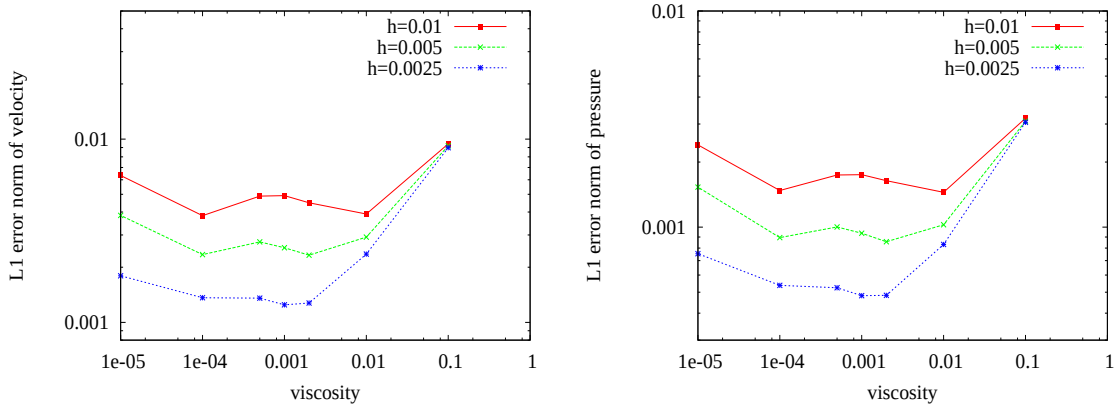

Figure 6: Sod shock tube problem - Error at $t = 1$, in L^1 norm (in space) for the velocity (left) and pressure (right) for three meshes, as a function of the artificial viscosity μ, with CFL= 9.6 (centered scheme).

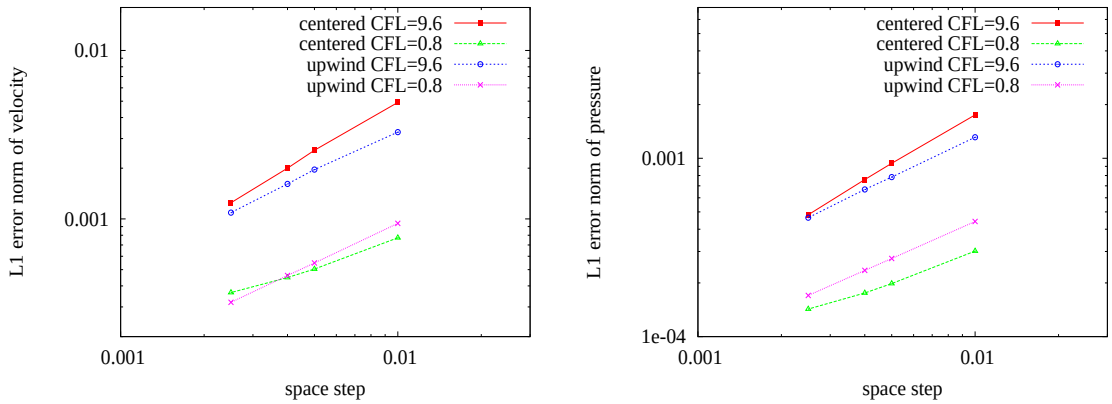

Figure 7: Sod shock tube problem - Error at $t = 1$, in L^1 norm (in space) for the velocity (left) and pressure (right), as a function of the mesh size, with fixed CFL numbers.

3.2 Two-fluid shock tube

We present here the numerical results for the two-fluid shock tube. The continuous problem is posed over $(-3, 2)$ and we use a computational rectangular domain $\Omega = [-3, 2] \times [0, 0.01]$. The equation of state is given by:

$$p = \frac{RT\rho_l \rho y}{\rho_\ell + \rho y - \rho},$$

where the parameters R and T are adjusted to produce $RT = 10$ and the liquid density is set constant $\rho_\ell = 0.8$. We perform two tests, where the initial left and right constant states are chosen in order to yield two different flow structures: a contact discontinuity (in both cases), propagating between two shock waves in the first case, and two rarefaction waves in the second one.

3.2.1 First case: shock-contact discontinuity-shock

The two initial constant states are given by:

$$\begin{pmatrix} \rho \\ \boldsymbol{u} \\ y \end{pmatrix}_L = \begin{pmatrix} 1 \\ 5 \\ 0.3 \end{pmatrix}, \qquad \begin{pmatrix} \rho \\ \boldsymbol{u} \\ y \end{pmatrix}_R = \begin{pmatrix} 2 \\ 1 \\ 0.8 \end{pmatrix}.$$

The same convergence behaviour as in the monophasic case (*i.e.* convergence of the upwind scheme or of the centered scheme with a residual viscosity and non-convergence of the centered scheme with $\mu = 0$) is observed here.

A numerical solution at $t = 0.1$ with 5000 meshes, $CFL = 0.75$, artificial viscosity $\mu = 0.002$ and centered advection term is plotted on Figure 8, together with the exact solution. Taking $v = 18.16$ (the velocity of the fastest wave, namely the right shock), the CFL number for these numerical parameters is CFL$=v\,\delta t/h = 0.75$.

Then we plot on Figure 9 the solution obtained at $t = 0.1$ with various CFL numbers, with the centered scheme, 2500 meshes and an artificial viscosity $\mu = 0.002$. We observe that the solution is qualitatively correct up to CFL of the order of 20, and then strongly deteriorates, showing in particular wild velocity and pressure oscillations at the contact discontinuity.

Finally, we assess the accuracy of the scheme as a function of the time and space step, with two constant CFL numbers, for the centered and upwind scheme; for the first option, the viscosity is given the constant value $\mu = 0.002$. For the centered scheme, the observed orders of convergence are about 1.5 and 1. at CFL$=$0.75 and 9 respectively, for both the velocity and the pressure; for ρ the order of convergence is 0.7 for both CFL numbers, and 0.5 for y. For the upwind scheme, the order of convergence is 1 for both the velocity and the pressure and 0.5 for ρ and y, at any CFL number.

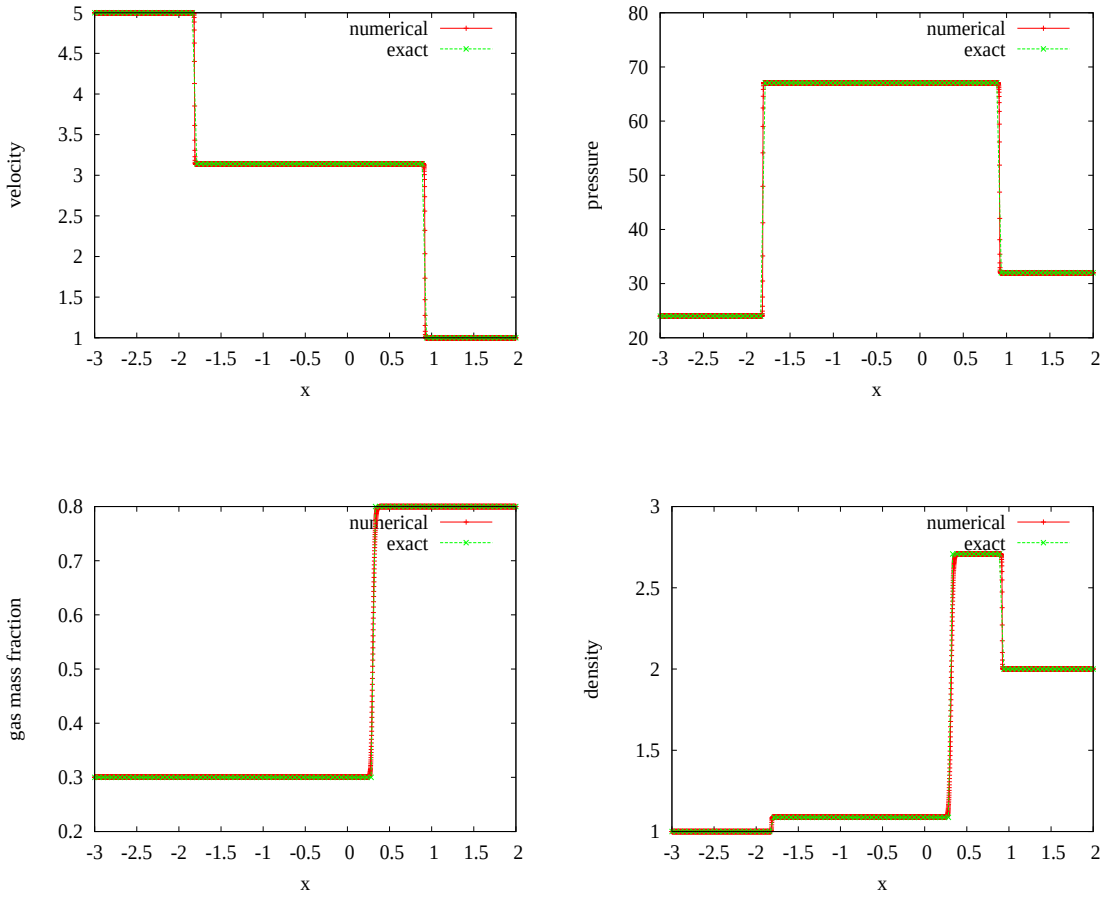

Figure 8: Two-phase test 1: shock-contact discontinuity-shock - Numerical solution at $t = 0.1$, with the centered scheme, 5000 meshes, CFL$==$ 0.75 and an artificial viscosity $\mu = 0.002$. Velocity (top left), pressure (top right), gas mass fraction (bottom left), density (bottom right)

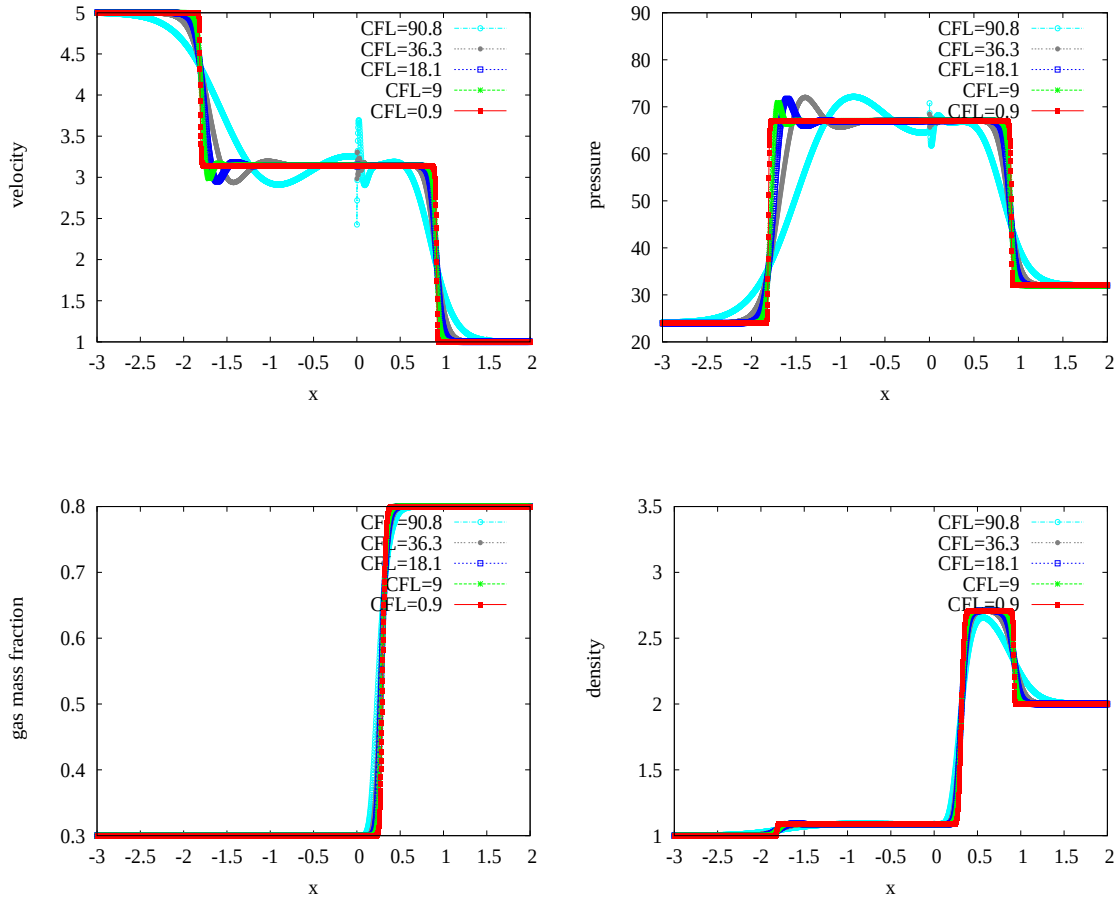

Figure 9: Two-phase test 1: shock-contact discontinuity-shock - Results obtained at $t = 0.1$ with the centered scheme, 2500 meshes and an artificial viscosity $\mu = 0.002$, for various CFL numbers. Velocity (top left), pressure (top right), gas mass fraction (bottom left), density (bottom right)

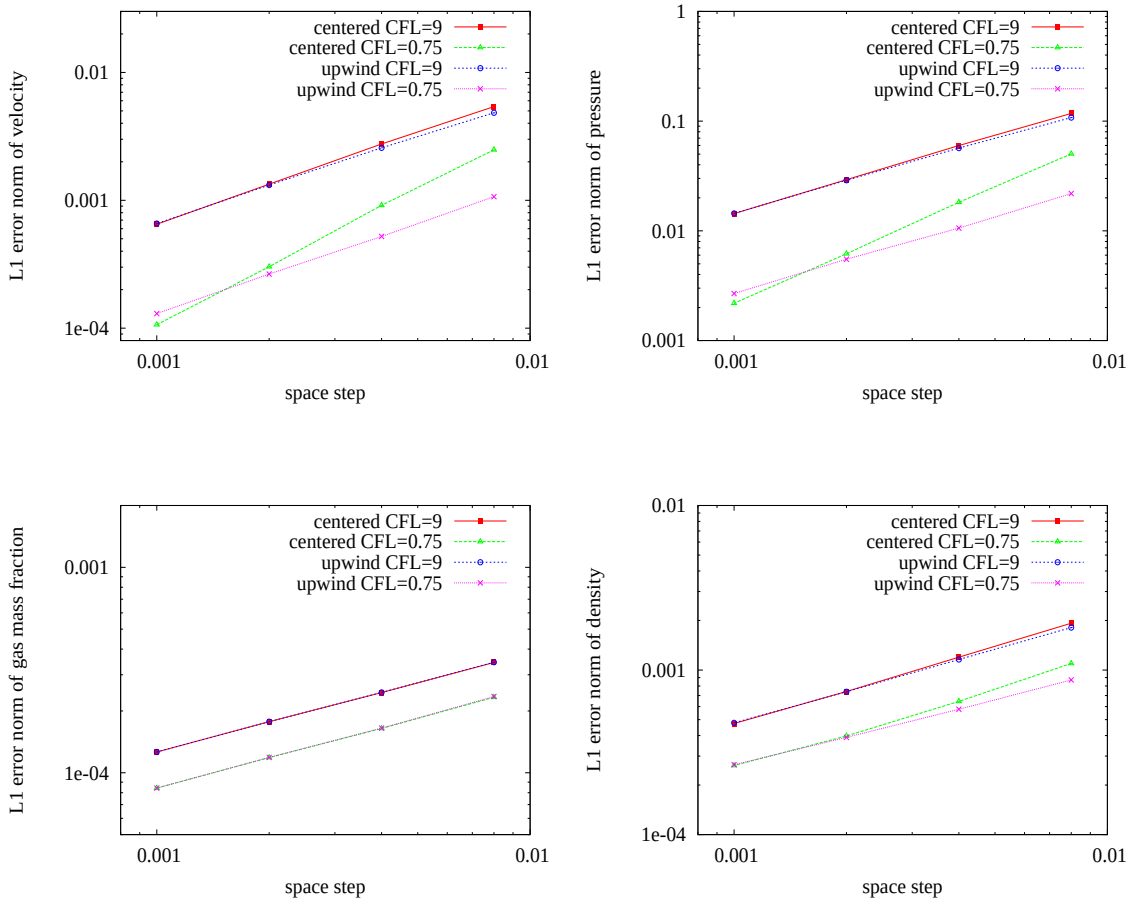

Figure 10: Two-phase test 1: shock-contact discontinuity-shock - Error at $t = 0.1$ in L^1 norm (in space) for the velocity (top left), pressure (top right), gas mass fraction (bottom left) and density (bottom right), as a function of the mesh size, with fixed CFL numbers.

3.2.2 Second case: rarefaction-contact discontinuity-rarefaction

We conclude this study by computing a diphasic test with rarefaction waves. The two initial constant states are given by:

$$\begin{pmatrix} \rho \\ \boldsymbol{u} \\ y \end{pmatrix}_L = \begin{pmatrix} 1 \\ 0 \\ 0.3 \end{pmatrix}, \qquad \begin{pmatrix} \rho \\ \boldsymbol{u} \\ y \end{pmatrix}_R = \begin{pmatrix} 2 \\ 2 \\ 0.8 \end{pmatrix}.$$

A numerical solution at $t = 0.1$, with 5000 meshes, $\delta t = 0.0001$, $\mu = 0.002$ and with the centered scheme presented on Figure 11. It coincides with the solution.

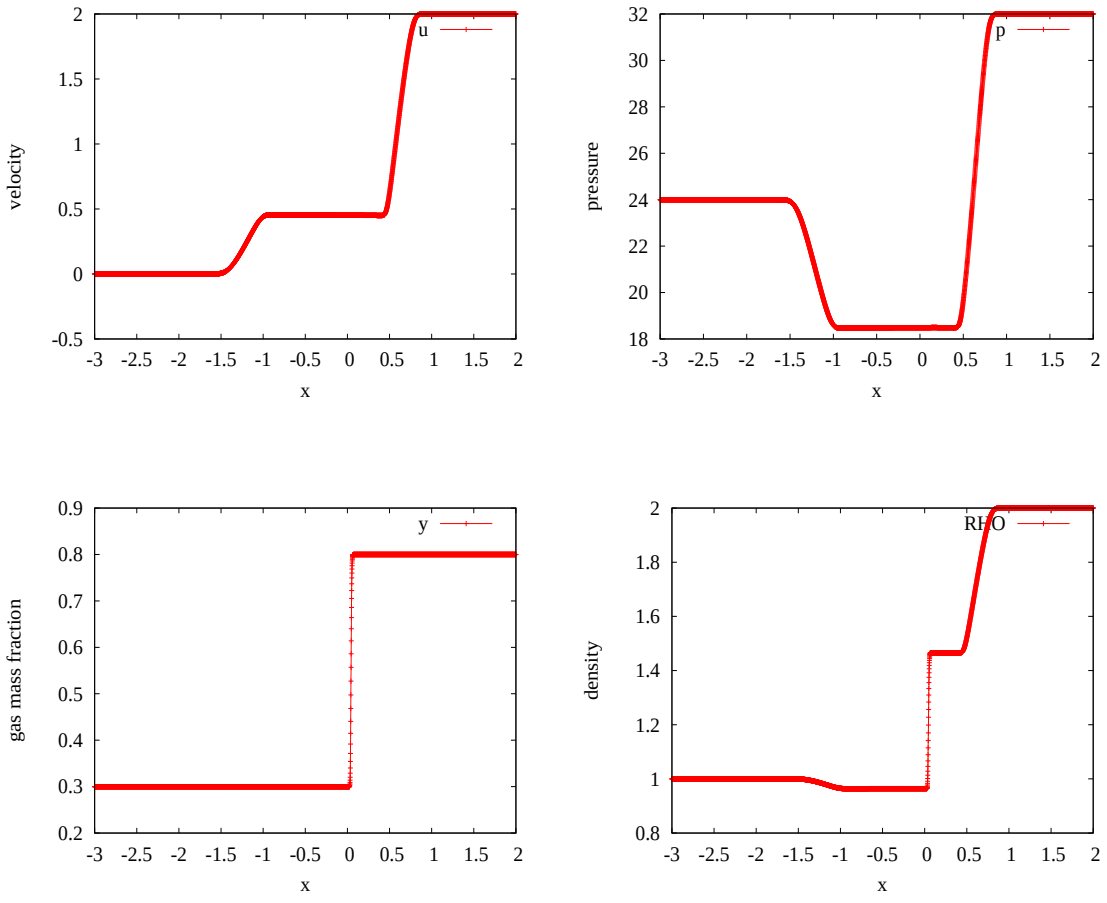

Figure 11: Two-phase test 2: rarefaction wave-contact discontinuity-rarefaction wave - Numerical solution at $t = 0.1$, with the centered scheme, 5000 meshes, $\delta t = 0.0001$ and an artificial viscosity $\mu = 0.002$. Velocity (top left), pressure (top right), gas mass fraction (bottom left), density (bottom right)

4 CONCLUSIONS

In this paper, we have assessed the capability of a scheme issued from the incompressible flow context, namely a pressure correction scheme, to compute discontinuous solutions of hyperbolic problems. Numerical tests show that, provided that a sufficient numerical dissipation is introduced in the scheme, it converges to the (weak) solution to the continuous problem; in addition, it shoes a satisfactory behaviour up to CFL numbers far greater than 1. Since the scheme boils down to usual projection schemes when the density is constant, this approach seems promising for the development of solvers robust with respect to the flow Mach number.

The present work should be extended in different ways. First, further numerical tests should address problems in more than one space dimension. Second, the artificial viscosity necessary for the scheme to converge could be monitored by *a posteriori* indicators, for instance following the ideas developped in [5]. Finally, the observed convergence should be conforted by theoretical arguments, even if a complete convergence proof seems out of reach, because of the lack of compactness of sequences of discrete solutions due, in particular, to the absence of diffusion terms.

REFERENCES

[1] G. Ansanay-Alex, F. Babik, J.-C. Latché, and D. Vola. An L2-stable approximation of the Navier-Stokes convection operator for low-order non-conforming finite elements. *to appear in International Journal for Numerical Methods in Fluids*, 2009.

[2] P. G. Ciarlet. Handbook of numerical analysis volume II : Finite elements methods – Basic error estimates for elliptic problems. In P. Ciarlet and J.L. Lions, editors, *Handbook of Numerical Analysis, Volume II*, pages 17–351. North Holland, 1991.

[3] T. Gallouët, L. Gastaldo, R. Herbin, and J.-C. Latché. An unconditionally stable pressure correction scheme for compressible barotropic Navier-Stokes equations. *Mathematical Modelling and Numerical Analysis*, 42:303–331, 2008.

[4] L. Gastaldo, R. Herbin, and J.-C. Latché. An unconditionally stable finite element-finite volume pressure correction scheme for the drift-flux model. *to appear in Mathematical Modelling and Numerical Analysis*, 2009.

[5] J.L Guermond and R. Pasquetti. Entropy-based nonlinear viscosity for Fourier approximations of conservation laws. *Comptes Rendus de l'Académie des Sciences de Paris – Série I – Analyse Numérique*, 346:801–806, 2008.

[6] F.H. Harlow and A.A. Amsden. A numerical fluid dynamics calculation method for all flow speeds. *Journal of Computational Physics*, 8:197–213, 1971.

[7] ISIS. A CFD computer code for the simulation of reactive turbulent flows. `https://gforge.irsn.fr/gf/project/isis`.

[8] D. Kuzmin and S. Turek. Numerical simulation of turbulent bubbly flows. In *3rd International Symposium on Two-Phase Flow Modelling and Experimentation, Pisa, 22-24 September*, 2004.

[9] B. Larrouturou. How to preserve the mass fractions positivity when computing compressible multi-component flows. *Journal of Computational Physics*, 95:59–84, 1991.

[10] F. Moukalled, M. Darwish, and B. Sekar. A pressure-based algorithm for multi-phase flow at all speeds. *Journal of Computational Physics*, 190:550–571, 2003.

[11] PELICANS. Collaborative development environment. `https://gforge.irsn.fr/gf/project/pelicans`.

[12] R. Rannacher and S. Turek. Simple nonconforming quadrilateral Stokes element. *Numerical Methods for Partial Differential Equations*, 8:97–111, 1992.

[13] B. Spalding. Numerical computation of multiphase flow and heat transfer. In *Recent Advances in Numerical Methods in Fluids – Volume 1*, pages 139–168, 1980.

[14] P. Wesseling. Principles of computational fluid dynamics. volume 29 of *Springer Series in Computational Mathematics*. Springer, 2001.